Preparation and structural characterization of Co/Au(001) superlattices

1993 J. Phys.: Condens. Matter 5 6515

(http://iopscience.iop.org/0953-8984/5/36/006)

J. Phys.: Condens. Matter 5 (1993) 6515–6524. Printed in the UK

Preparation and structural characterization of Co/Au(001) superlattices

Lianjun Wu†, Kazuhiko Shintaku†§, Teruya Shinjo† and Noriaki Nakayama‡‖
† Institute for Chemical Research, Kyoto University, Uji 611, Japan
‡ Department of Chemistry, Faculty of Science, Kyoto University, Kyoto 606, Japan

Received 18 March 1993, in final form 3 June 1993

Abstract. By means of an electron beam deposition technique under ultrahigh vacuum, Co/Au(001) superlattices were prepared on GaAs(001) substrates with a 500 Å thick Au(001) buffer layer. The superlattices were characterized by reflection high-energy electron diffraction (RHEED), and x-ray diffraction. We found that well defined single-crystalline Co/Au(001) superlattices can be obtained only for samples with Co layer thickness below about 10 Å. The results from x-ray diffraction measurements indicate a slightly strained BCC structure for Co layers with the lattice constants $a^{\parallel} = 2.88 \pm 0.01$ Å in the film plane and $a^{\perp} = 2.78 \pm 0.02$ Å along the growth direction.

1. Introduction

The molecular beam epitaxy technique has been widely used to grow new phases of materials which do not exist in nature [1–4]. Since the pioneering work by Prinz [1] on the epitaxial growth of metastable BCC Co on GaAs(110) substrates, many studies to characterize the structure and the magnetic properties of BCC Co have been reported [5–7]. The magnetic moment per Co atom in a BCC lattice structure is theoretically predicted to be $1.68\mu_B$ by Moruzzi *et al* [8]. However a value of $1.53\mu_B$ was obtained from experiment [1]. Later investigations by means of x-ray and polarized neutron reflection have displayed a distribution of Co magnetic moment as a function of the position of Co atoms along the growth direction [6]. It was pointed out that the imperfect crystalline quality of the Co layer and a chemical reaction between the Co and substrate were responsible for the discrepancy between experiments and calculations [6]. We note that besides GaAs substrates, Au(001) substrates can also be used to stabilize the metastable BCC Co phase. Thin films of BCC Fe can be grown epitaxially on Au(001) layers due to the negligible misfit between BCC Fe and FCC Au when Fe BCC[100]‖Au FCC[100] in the film plane [9]. According to the calculation by Moruzzi *et al* [8], the lattice constant for BCC Co ($a_{Co} = 2.80$ Å) is very near to that for BCC Fe ($a_{Fe} = 2.88$ Å), and the mismatch in the film plane between Co BCC[110] and Au FCC[100] is 2.9% when Co BCC[110]‖Au FCC[100]. Also, the binary phase diagram for the Co–Au system indicates that the two elements are almost insoluble in each other below 700 K and that there is no intermetallic compound between them [10]. Thus, chemical reaction can be avoided when Co layers are epitaxially grown on Au layers. In this work, we report the preparation and the structural characterization of the Co/Au(001) superlattices.

§ Present address: Advanced Thin Film Research Laboratories, Tokyo Research Centre, Teijin Ltd, 4-3-2 Asahigaoka, Hino, Tokyo 191, Japan.

‖ Present address: Department of Advanced Materials Science and Engineering, Faculty of Engineering, Yamaguchi University, Ube 755, Japan.

0953-8984/93/366515+10$07.50

2. Experimental details

The samples were prepared in an ultrahigh-vacuum chamber equipped with a reflection high-energy electron diffraction (RHEED) apparatus. A substrate of GaAs(001) single crystal was chemically etched in a solution composed of H_2SO_4, H_2O_2, and H_2O (3:1:1) before being transferred into the chamber. It was then heated to 300 °C for 3 h under vacuum. Prior to the deposition of the superlattices, an Au buffer layer of 500 Å was deposited at a substrate temperature of 200 °C. The superlattices were prepared at a substrate temperature of 50 °C. The deposition rate for Au was about 0.3 Å s^{-1}, and that for Co was about 0.2 Å s^{-1}. Two series of samples were prepared. In the first series the Co layer thickness t_{Co} was kept at 9.4 Å while the Au layer thickness t_{Au} was varied by 1 Å from 22 Å to 28 Å. In the second series t_{Co} was varied from about 5 Å to 19 Å while t_{Au} was held constant at 28 Å. These layer thicknesses for Co and Au are those calibrated with x-ray diffraction measurements, which are described below. The number of Co/Au bilayers was 20 for all samples and a final 50 Å thick Au cover layer was deposited for protection against oxidation of the Co. The *in situ* RHEED patterns were recorded on photographic films during the sample preparation. Small-angle, high-angle and off-axis x-ray diffraction measurements were performed using a computer-controlled four-circle x-ray diffractometer. Cu Kα radiation ($\lambda = 1.542$ Å) from a rotating-anode source was used.

3. Results and discussion

3.1. RHEED observations

The orientation of the 500 Å Au buffer layer deposited on the GaAs(001) single-crystal substrate was determined from the RHEED observations and the high-angle x-ray diffraction measurements. We found that Au[110]‖GaAs[110], Au(001)‖GaAs(001) for all samples. This orientation is the same as that reported previously by Okuyama [11] since we have followed similar preparation conditions. The epitaxial growth of Co/Au(001) superlattices has been investigated *in situ* by RHEED observations. Figure 1 shows the RHEED patterns taken after the depositions of the Au buffer layer and the various Co layer thicknesses indicated in the figure caption. The sharp streak pattern observed from the 500 Å Au buffer layer indicates good crystalline quality. Streak features with the same spacing as that of the Au buffer layer were observed after the deposition of Co layers. The RHEED patterns became gradually blurred with the continuous deposition of Co, but their distinct features indicate that the Co grows epitaxially up to the thickest Co layer ($t_{Co} = 24$ Å) we have deposited in this work.

3.2. Small- and high-angle x-ray diffraction measurements

Small-angle and high-angle θ–2θ x-ray diffraction profiles were measured for each sample. Figure 2 shows the small-angle x-ray diffraction patterns for three samples in the first series, with $t_{Au} = 22$ Å, 25 Å, 28 Å and $t_{Co} = 9.4$ Å. Bragg peaks up to a very high order were observed. We conclude that the interdiffusion at the interface of Co and Au is very limited, since its presence would cause a fast decrease of higher-order Bragg peaks. In order to avoid the refraction effect on the Bragg peak positions, only Bragg peaks above 6° were used to determine the actual modulation wavelength Λ in each superlattice. Figure 3 is the plot of the observed modulation wavelength Λ versus the designed Au layer thickness t_{Au}. The straight line in the figure is the least-squares-fitted result. The slope of this line is 1.00,

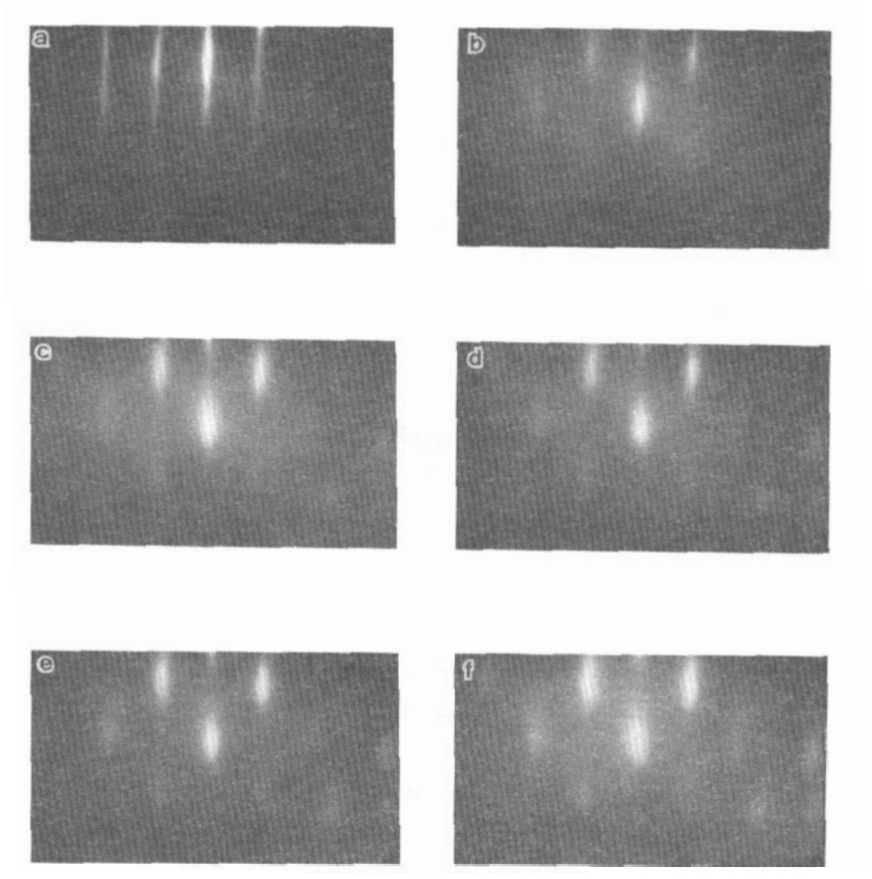

Figure 1. RHEED patterns recorded with the incident electron beam along GaAs[110] for Co layers deposited on a 500 Å Au buffer layer: (*a*) $t_{Co} = 0.0$ Å; (*b*) $t_{Co} = 4.7$ Å; (*c*) $t_{Co} = 9.4$ Å; (*d*) $t_{Co} = 14.1$ Å; (*e*) $t_{Co} = 18.8$ Å; (*f*) $t_{Co} = 23.5$ Å.

indicating excellent agreement of the actual t_{Au} with the designed ones. The intercept on the Λ axis gives the Co layer thickness in each sample, which is equal to 9.40 ± 0.05 Å. This value is used to estimate the lattice spacing along the growth direction. Non-monotonic changes in the peak intensity were observed in the small-angle x-ray diffraction patterns shown in figure 2. They indicate that the layer thickness ratios of Co to Au agree well with the designed ones. According to a step-model calculation [12], the $(m + 1)$th Bragg diffraction peak would become extinct when the layer thickness ratio of two constituents is $m : 1$ or $1 : m$. For a sample with $t_{Au} = 28$ Å, the designed layer thickness ratio of Au to Co is 2.98 : 1, very close to 3 : 1. Therefore, in the observed small-angle x-ray diffraction pattern for this sample, the fourth peak is very weak. The high-angle x-ray diffraction patterns for all these samples show many satellite peaks around the Au(002) reflection. One of these patterns measured for the sample with $t_{Au} = 28$ Å is shown in figure 4.

Figure 4 shows observed x-ray diffraction patterns for the four samples in the second series with $t_{Co} = 4.7$ Å, 9.4 Å, 14.1 Å, 18.8 Å and $t_{Au} = 28$ Å. Sharp diffraction peaks in the small-angle range were observed for all the samples. However, the high-angle x-ray diffraction patterns display remarkable variations with increase of t_{Co}. For samples with thicker Co layers, the satellite peaks are broadened. The satellite peak intensities decreased

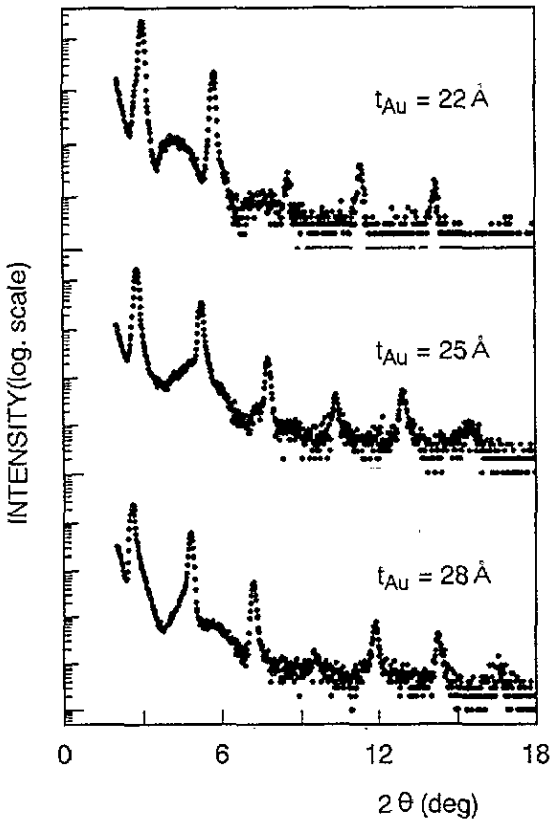

Figure 2. Small-angle x-ray diffraction patterns plotted on a logarithmic scale for [Co(9.4 Å)/Au(22 Å)]$_{20}$, [Co(9.4 Å)/Au(25 Å)]$_{20}$, and [Co(9.4 Å)/Au(28 Å)]$_{20}$. The Au layer thicknesses t_{Au} are shown in the figure.

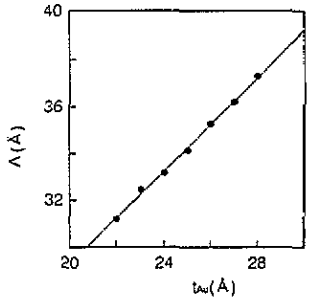

Figure 3. The observed modulation wavelength Λ plotted versus the designed Au layer thickness t_{Au}. The straight line is the least-squares-fitted result.

drastically for the sample with t_{Co} = 14.1 Å, and almost disappeared for the sample with t_{Co} = 18.8 Å. Since the x-ray diffraction pattern in the small-angle range originated mainly from the composition modulation along the growth direction, the x-ray diffraction patterns in figure 4 indicate that the designed multilayered structures were fabricated. However, in the high-angle range, with increase of t_{Co} the broadening in peak width and the decrease in peak intensity mean that the structural coherence deteriorated because of the increase of roughness, especially the continuous fluctuation in lattice spacing as has been pointed out in the literature [13]. Therefore, the above results indicate that the well defined single-crystalline Co/Au(001) superlattices can be obtained only for t_{Co} below about 10 Å.

3.3. Measurements of in-plane lattice constants

Estimation of the in-plane lattice constants of both Au and Co layers from x-ray diffraction measurements is very important to understand the structure of superlattices. However, because of the strong x-ray absorption due to the thick GaAs substrate, it was difficult to measure the in-plane lattice constants in the transmitting geometry. Instead, we performed off-axis x-ray scans to determine the in-phase lattice constants. In the off-axis x-ray diffraction measurements, the diffracted x-ray intensities were recorded versus Q_x and Q_z instead of 2θ as in the conventional measurements. Here Q_z is defined as the scattering

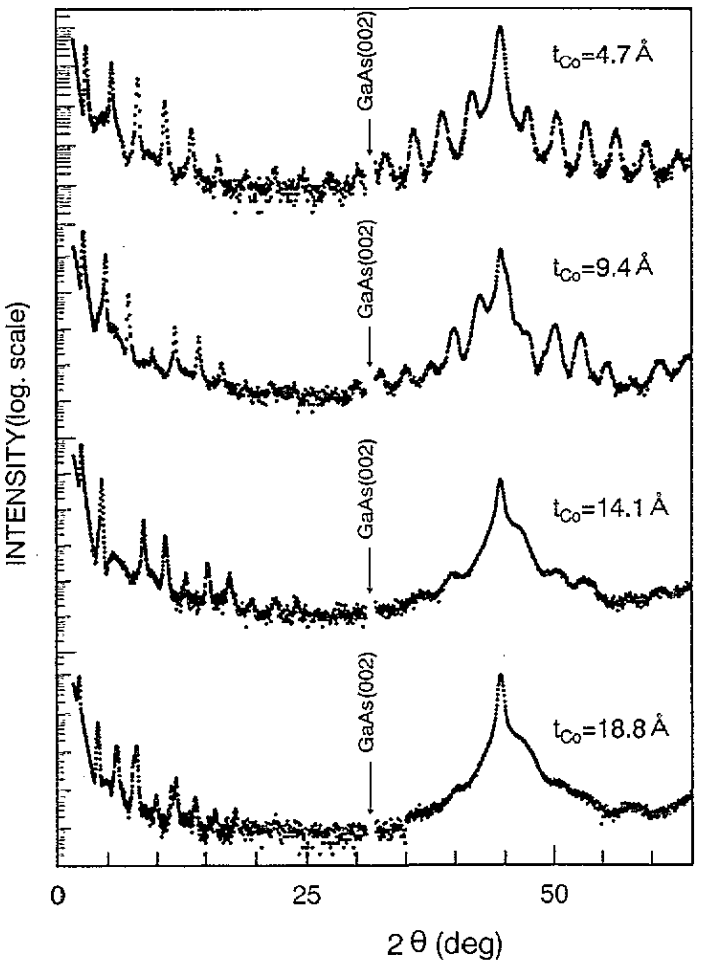

Figure 4. X-ray diffraction patterns plotted on a logarithmic scale for [Co(4.7 Å)/Au(28 Å)]$_{20}$, [Co(9.4 Å)/Au(28 Å)]$_{20}$, and [Co(14.1 Å)/Au(28 Å)]$_{20}$, and [Co(18.8 Å)/Au(28 Å)]$_{20}$. The Co layer thicknesses t_{Co} are shown in the figure.

vector component directed perpendicular to the film plane and Q_x the in-plane component adjusted to be parallel to the Au[110] direction. The off-axis-scan technique has been used to evaluate lattice strains and characterize the three-dimensional structures of superlattice films, such as the FCC/HCP stacking disorder for superlattices [14–18]. A detailed description of the off-axis geometry used in this study can be found elsewhere [19]. Several Q_z-scan profiles were measured around the FCC 113 reciprocal point. By contour plotting these Q_z scans at different Q_x, the in-plane lattice constants for both layers can be determined from the positions of superlattice peaks on the Q_x axis. Figure 5 shows the logarithmic contour plots for three samples with t_{Au} = 22 Å, 25 Å, and 28 Å. A very strong diffraction peak of the FCC 113 reflection from the Au buffer layer was observed at its bulk position ($Q_x = 2.180 \pm 0.005$ Å^{-1}, $Q_z = 4.620 \pm 0.005$ Å^{-1}), insuring the precision of the measurements. The peak positions of superlattice reflections along Q_x are indicated by the vertical broken lines in each plot. They are the same for all of these samples

($Q_x = 2.180 \pm 0.005$ Å^{-1}) and are coincident with that of the Au buffer layer. This is in good agreement with our RHEED observations. Therefore, from this Q_x peak value, the in-plane lattice constants for Co layers and Au layers are determined as $d^{\parallel}_{Au} = d^{\parallel}_{Co} = 2.88 \pm 0.01$ Å. It is obvious that the result for Au is the d^{110} (2.88 Å) of FCC bulk Au, while that for Co is much closer to d^{100} (2.80 Å) of BCC Co than to d^{110} (2.50 Å) of FCC Co. So the observed in-plane lattice constant indicates a BCC structure for Co layers.

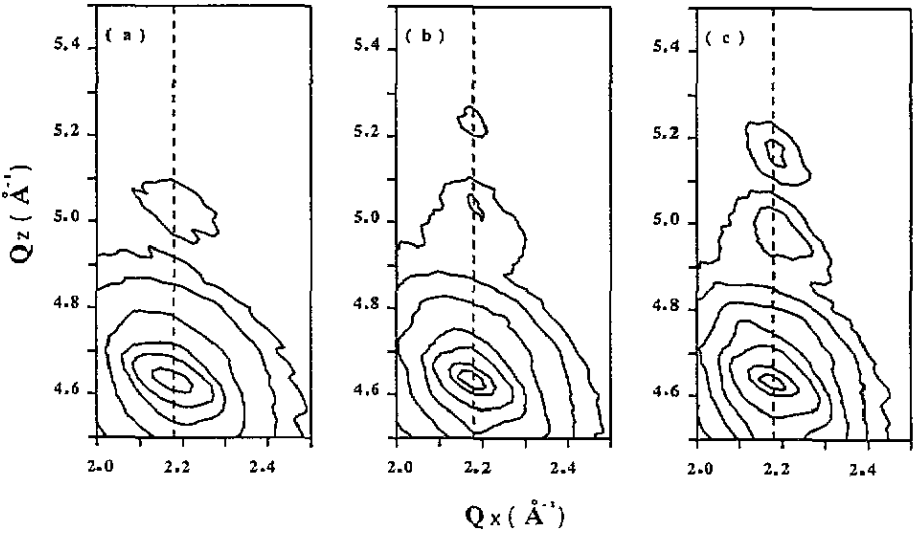

Figure 5. Logarithmic contour plots of the off-axis x-ray diffraction measurements around the Au and Co/Au(113) reflection for (*a*) [Co(9.4 Å)/Au(22 Å)]$_{20}$; (*b*) [Co(9.4 Å)/Au(25 Å)]$_{20}$; and (*c*) [Co(9.4 Å)/Au(28 Å)]$_{20}$. The vertical broken lines indicate the Q_x value at peak positions. Peaks at $(Q_x, Q_z) = (2.18$ Å$^{-1}, 4.62$ Å$^{-1})$ are Au(113) peaks from buffer layers and the other peaks are from the Co/Au(001) superlattices.

3.4. Estimate of lattice spacings in the growth direction

In this section, we describe the estimate of the lattice spacings along the growth direction for the Co and Au layers. The lattice constant of Co layers along the growth direction can be obtained by analysing the fundamental reflection peak positions in θ–2θ x-ray diffraction patterns for the first series of samples. As from a theoretical analysis [20, 21], the fundamental reflection in a usual θ–2θ x-ray diffraction pattern gives the average lattice spacing of the two constituents, that is:

$$d_0 = (n_{Au} d^{002}_{Au} + n_{Co} d^{002}_{Co})/(n_{Au} + n_{Co}) \tag{1}$$

where n_{Au}, n_{Co} represent the average numbers of atomic planes contained in one Au layer and one Co layer and d^{002}_{Au}, d^{002}_{Co} the lattice spacings in each layer, respectively. Since $\Lambda = (n_{Au} d^{002}_{Au} + n_{Co} d^{002}_{Co})$, $t_{Au} = n_{Au} d^{002}_{Au}$, and $t_{Co} = n_{Co} d^{002}_{Co}$, we therefore obtain a very simple expression for Λ/d_0:

$$\Lambda/d_0 = (n_{Au} + n_{Co}) = (t_{Au}/d^{002}_{Au} + t_{Co}/d^{002}_{Co}). \tag{2}$$

Therefore, if d_{Co}^{002} and d_{Au}^{002} are assumed to be sample independent, which is reasonable here since t_{Co} has been kept constant and t_{Au} is very thick, then a plot of Λ/d_0 versus t_{Au} should be a straight line. The lattice spacing along the growth direction for the Au layer can be obtained from the slope $1/d_{Au}^{002}$ and that for the Co layer can be determined from the intercept t_{Co}/d_{Co}^{002} on the Λ/d_0 axis with the t_{Co} value determined as discussed in section 3.2. Before performing this analysis, it is necessary to index the fundamental reflection peak. This is not straightforward in this case since the lattice spacings are unknown parameters to be determined. In order to uniquely determine the fundamental reflection peak, diffraction-peak positions in the x-ray diffraction patterns measured along Q_z at $Q_x = 0.0$ Å^{-1} (which is the same as a θ–2θ scan) were compared with those measured at $Q_x = 2.180$ Å^{-1}. Each pattern has a fundamental diffraction peak. The Q_z value of the Co/Au(002)$_0$ fundamental peak is related to the Co/Au(113)$_0$ fundamental peak by a factor of 1.5 because of the relation $d^{002} = 1.5d^{003}$. Figure 6 shows an example of the two diffraction patterns measured for the sample [Co(9.4 Å)/Au(28 Å)]$_{20}$. In this figure, the Au(002) and Au(113) peaks from the buffer layer and the Co/Au(002)$_0$ and Co/Au(113)$_0$ fundamental peaks as well as other satellite peaks from the superlattice are indicated. Having determined the fundamental reflection peaks, we obtained d_0 values from these fundamental peaks for each sample plotted Λ/d_0 versus t_{Au} as shown in figure 7. The lattice spacing d_{Au}^{002} along the growth direction for the Au layer is evaluated from the slope of the straight line, and it is $d_{Au}^{002} = 2.03 \pm 0.01$ Å (or $a_{Au}^{\perp} = 4.06$ Å), which is reasonable compared to its bulk value ($a = 4.08$ Å). Besides, from the intercept on the d_0 axis of the least-squares-fitted straight line in the figure, the lattice spacing along the growth direction for the Co layers is found to be $d_{Co}^{002} = 1.39 \pm 0.01$ Å (or $a^{\perp} = 2.78$ Å). As d^{002} for FCC Co is 1.77 Å but 1.40 Å for BCC Co, the lattice constant along the growth direction also indicates a BCC structure for Co layers.

Table 1. Structural parameters obtained from the profile-fitting method. For the meaning of each parameter, see the text.

	Sample		
Parameters	(*a*) [Co(9.4 Å)/Au(22 Å)]$_{20}$	(*b*) [Co(9.4 Å)/Au(25 Å)]$_{20}$	(*c*) [Co(9.4 Å)/Au(28 Å)]$_{20}$
Λ (Å)	31.4	34.5	37.5
a_{Au}^{002} (Å)	2.03	2.03	2.04
d_{Co}^{002} (Å)	1.38	1.38	1.39
t_{Au} (Å)	22.0	25.0	28.0
t_{Co} (Å)	9.28	9.28	9.27
Δt_{Au} (Å)	1.52	1.40	1.41
Δt_{Co} (Å)	0.93	0.60	0.66
R_{log}[a] (%)	14	18	17

[a] $R_{log} = \sum |\log[I_{cal}(Q_i)] - \log[I_{obs}(Q_i)]| / \sum \log[I_{obs}(Q_i)]$.

The lattice spacings along the growth direction for Co and Au layers have also been estimated using a computer fitting method developed by Nakayama *et al* [19]. Structural parameters such as layer thicknesses t_{Au} and t_{Co}, lattice spacings d_{Au}^{002} and d_{Co}^{002}, the number N of coherent unit layers and the fluctuations Δt_{Au}, Δt_{Co} in layer thicknesses for the superlattice and the buffer layer were determined from fitting the θ–2θ x-ray diffraction profiles measured for each sample. In the fitting procedure (1) the variations in the composition and the lattice spacing along the growth direction were approximated to vary stepwise at interfaces (step model); (2) a discrete Gaussian fluctuation in the number of

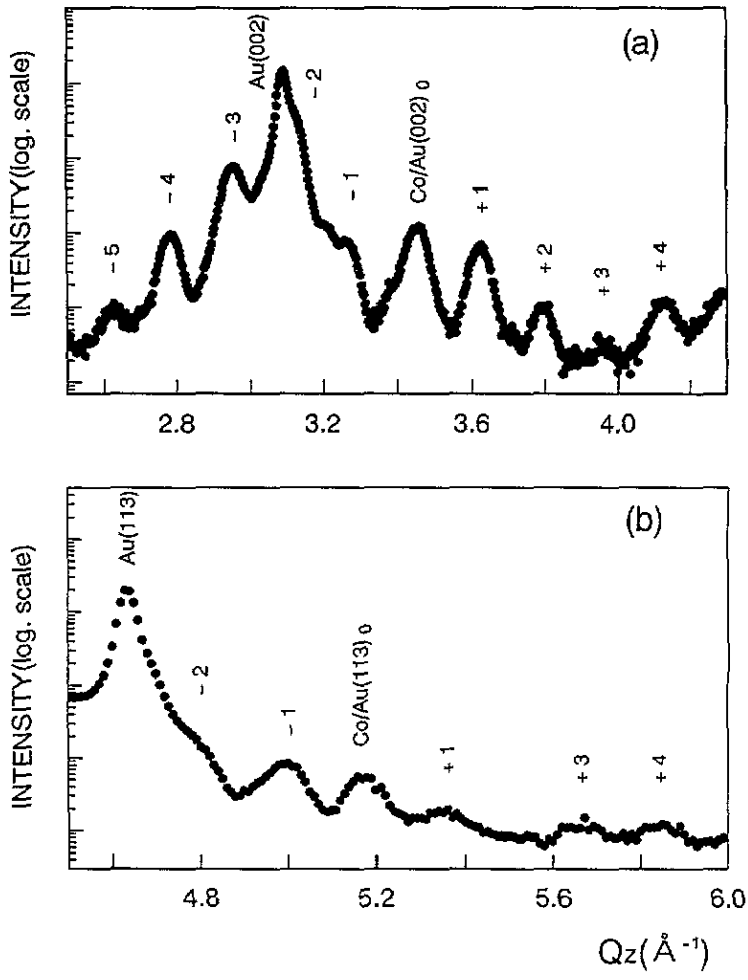

Figure 6. X-ray diffraction patterns for [Co(9.4 Å)/Au(28 Å)]$_{20}$: (*a*) Q_z scan at $Q_x = 0$, which is the same as the ordinary θ–2θ scan; (*b*) Q_z scan at $Q_x = 2.180$ Å^{-1}.

atomic planes was assumed; (3) the atomic number densities σ_{Au} and σ_{Co} in the film plane for both constituents were set equal ($\sigma_{Au} = \sigma_{Co} = 0.120$ Å^{-2}) according to RHEED observation and off-axis x-ray diffraction measurements; and (4) the profile shape was assumed to be of modified Lorentzian type ($L(Q)^{\alpha}$), where α was fixed to be 2.0. A more detailed description of the fitting method has been presented in [19]. Figure 8 shows the observed and fitted profiles for three samples: [Co(9.4 Å)/Au(22 Å)]$_{20}$, [Co(9.4 Å)/Au(25 Å)]$_{20}$, and [Co(9.4 Å)/Au(28 Å)]$_{20}$. The final parameters from the fitting are summarized in table 1. The layer thicknesses for both constituents as determined in section 3.1 were reproduced. The lattice spacings for the Co and Au layers obtained from this profile-fitting method are $d_{Co}^{002} = 1.38 \pm 0.01$ Å and $d_{Au}^{002} = 2.04 \pm 0.01$ Å, respectively, which are in good agreement with those obtained in our analysis of average lattice spacing described earlier in this section. The R_{log} factor listed in table 1 provides a numerical estimate of the reliability for the present fitting method. Similar R_{log} values to that presented in [19] are achieved.

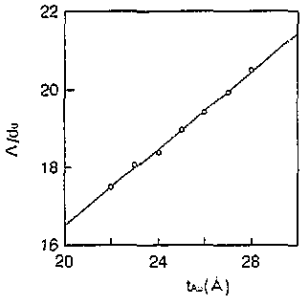

Figure 7. Plot of Λ/d_0 versus t_{Au}. The intercept of the least-squares-fitted line on Λ/d_0 is equal to the value of t_{Co}/d_{Co}^{002} for the Co layers, and the slope of the straight line is equal to the reciprocal value of the lattice constant d_{Au}^{002} for the Au layers along the growth direction.

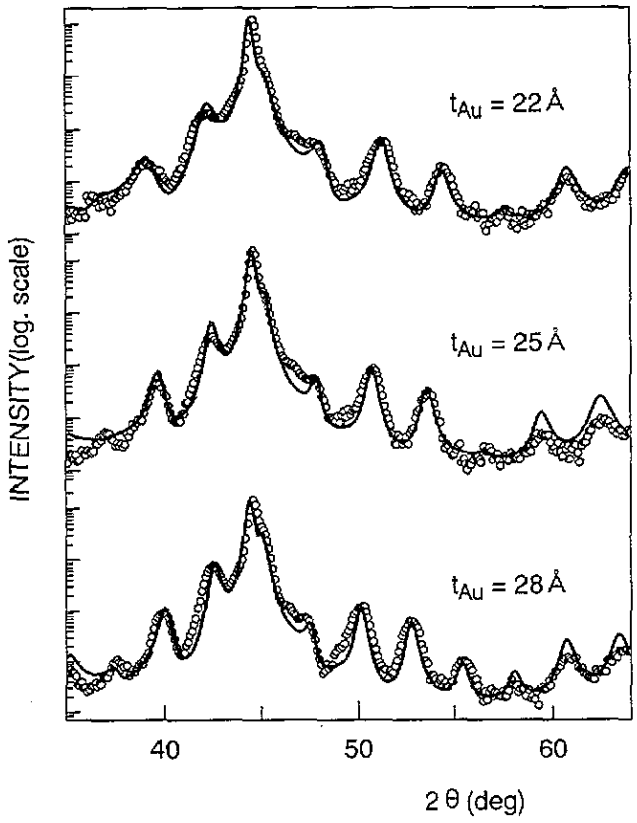

Figure 8. Measured (O) and fitted (——) θ–2θ x-ray diffraction profiles in the high-angle range for (*a*) [Co(9.4 Å)/Au(22 Å)]$_{20}$, (*b*) [Co(9.4 Å)/Au(25 Å)]$_{20}$, and (*c*) [Co(9.4 Å)/Au(28 Å)]$_{20}$. They are plotted on a logarithmic scale. The profile-fitting procedure is described in the text.

3.5. Structural aspects of Co layers

The present x-ray diffraction measurements indicate that the lattice constants for the Au layers in the superlattices ($d_{Au}^{110} = 2.88 \pm 0.01$ Å, $d_{Au}^{002} = 2.03 \pm 0.01$ Å) are nearly the same as bulk ones. This observation is reasonable since the layer thickness of Au layers was always much thicker than that of the Co layers in the Co/Au(001) superlattices. The results for Co layers show a small difference between the in-plane lattice constant and that along the growth direction ($a_{Co}^{\parallel} = 2.88 \pm 0.01$ Å, $a_{Co}^{\perp} = 2.78 \pm 0.02$ Å). As has been pointed out in section 3.4, these lattice constants indicate a BCC structure for the Co layers rather than an FCC structure. The ratio of these two lattice constants, which is $a_{Co}^{\perp}/a_{Co}^{\parallel} = 0.965$, also shows that the Co layers in Co/Au(001) superlattices have been grown in a slightly strained BCC structure. Comparing with the theoretical lattice constant for BCC Co presented in [8], these Co layers are expanded by 2.9% in the film plane and contracted by 0.7% along the growth direction of the film. The epitaxial orientation relation between BCC Co and FCC Au layers was Co(002)‖Au(002) along the growth direction and Co[100]‖Au[110] in the film plane, which is the same as reported between BCC Fe and FCC Au [9, 11].

4. Summary

We have prepared epitaxial Co/Au(001) superlattices with high crystalline quality on GaAs(001) single-crystal substrates. From the x-ray diffraction measurements and RHEED observations we found that well defined single-crystalline Co/Au(001) superlattices can be obtained only for t_{Co} below about 10 Å. We succeeded in determining the lattice constants, both in the film plane and along the growth direction, for Co layers in Co/Au(001) superlattices. Measurements of the magnetization and magnetoresistance effect of the Co/Au(001) superlattices are under way and will be reported in a separate paper.

Acknowledgments

The authors would like to thank Drs N Hosoito and K Mibu for collaboration. Thanks are also due to Dr B Engel, University of Arizona, for helpful discussion. This work has been supported by a grant-in-aid for scientific research on priority areas (No 04224103) from the Ministry of Education, Science and Culture, Japan.

References

[1] Prinz G A 1985 *Phys. Rev. Lett.* **54** 1051
[2] Wang Z Q, Lu S H, Li Y S, Jona F and Marcus P M 1987 *Phys. Rev.* B **35** 9322
[3] Heinrich B, Purcell S T, Dutcher J R, Urquhart K B, Cochran J F and Arrott A S 1988 *Phys. Rev.* B **38** 12 879
[4] Gutierrez C J, Wieczorek M D, Qiu Z Q, Tang H and Walker J C 1991 *J. Magn. Magn. Mater.* **93** 369
[5] Idzerda Y U, Elam W T, Jonker B T and Prinz G A 1989 *Phys. Rev. Lett.* **62** 2480
[6] Bland J A C, Bateson R D, Riedi P C, Graham R G, Lauter H J, Penfold J and Shackleton C 1991 *J. Appl. Phys.* **69** 4989
[7] Bland J A C, Blundell S J, Gester M, Bateson R D, Singleton J, Cox U J, Lucas C A, Poon W C K and Penfold J 1992 *J. Magn. Magn. Mater.* **115** 359
[8] Moruzzi V L, Marcus P M, Schwarz K and Mohn P 1986 *J. Magn. Magn. Mater.* **54** 955
[9] Vermaak J S, Snyman L W and Auret F D 1977 *J. Cryst. Growth* **42** 132
[10] Massalski T B, Murray J L, Bennett L H, Baker H and Kacprzak L (ed) 1986 *Binary Alloy Phase Diagrams* vol 1 (Metals Park, OH: American Society for Metals)
[11] Okuyama T 1991 *Japan. J. Appl. Phys.* **30** 2053
[12] Underwood J H and Barbee T W Jr 1981 *Appl. Opt.* **20** 3027
[13] See, for example, Fullerton E E, Schuller I K, Vanderstraeten H and Bruynseraede Y 1992 *Phys. Rev.* B **45** 9292 and references therein
[14] Gyorgy E M, McWhan D B, Dillon J F Jr, Walker L R and Waszczak J V 1982 *Phys. Rev.* B **25** 6739
[15] Zheng J Q, Ketterson J B and Felcher G P 1982 *J. Appl. Phys.* **53** 3624
[16] Lee C H, Hui He, Lamelas F, Vavra W, Uher C and Clarke R 1989 *Phys. Rev. Lett.* **62** 653
[17] Lamelas F J, Lee C H, Hui He, Vavra W and Clarke R 1989 *Phys. Rev.* B **40** 5837
[18] v d Hoogenhof W W and Ryan T W 1993 *J. Magn. Magn. Mater.* **121** 88
[19] Nakayama N, Okuyama T and Shinjo T 1993 *J. Phys.: Condens. Matter* **5** 1173
[20] Engel B N, England C D, Van Leeuwen R A, Wiedmann M H and Falco C M 1991 *J. Appl. Phys.* **70** 5873
[21] Fujii Y 1987 *Metallic Superlattices* ed T Shinjo and T Takada (Amsterdam: Elsevier)